Enhanced innate immune suppression by SARS-CoV-2 Omicron subvariants BA.4 and BA.5

Ann-Kathrin Reuschl[1], Lucy G. Thorne[1], Matthew V.X. Whelan[1], Dejan Mesner[1], Roberta Ragazzini[2], Giulia Dowgier[1], Nathasha Bogoda[1], Jane L. E. Turner[1], Wilhelm Furnon[3], Vanessa M. Cowton[3], Giuditta de Lorenzo[3], Paola Bonfanti[1,2], Massimo Palmarini[3], Arvind H. Patel[3], Clare Jolly[1*] and Greg. J. Towers[1*]

[1]Division of Infection and Immunity, University College London, WC1E 6BT London, United Kingdom. [2]Epithelial Stem Cell Biology and Regenerative Medicine Laboratory, The Francis Crick Institute, London, NW1 1AT, United Kingdom. [3]MRC-University of Glasgow Centre for Virus Research, Glasgow, G61 1QH, United Kingdom.

* These authors contributed equally.

Co-Corresponding authors:

Ann-Kathrin Reuschl a.reuschl@ucl.ac.uk

Clare Jolly c.jolly@ucl.ac.uk

Greg J. Towers g.towers@ucl.ac.uk

Keywords: SARS-CoV-2, VOC, Omicron, COVID-19, innate immunity, Orf6

SARS-CoV-2 adaptation to its human host is evidenced by the emergence of new viral lineages with distinct genotypic and phenotypic characteristics, termed variants of concern (VOCs). Particular VOCs have become sequentially dominant globally (Alpha, Delta, Omicron) with each evolving independently from the ancestral Wuhan strain. Omicron is notable for its large number of spike mutations[1] found to promote immune escape and re-infection[2]. Most recently, Omicron BA.4 and BA.5 subvariants have emerged with increasing levels of adaptive immune escape threatening vaccine effectiveness and increasing hospitalisations[1,3–12]. Here, we demonstrate that the most recent Omicron variants have enhanced capacity to antagonise or evade human innate immune defenses. We find Omicron BA.4 and BA.5 replication is associated with reduced activation of epithelial innate immune responses versus earlier BA.1 and BA.2 subvariants. We also find enhanced expression of innate immune antagonist proteins Orf6 and N, similar to Alpha, suggesting common pathways of human adaptation and linking VOC dominance to improved innate immune evasion. We conclude that Omicron BA.4 and BA.5 have combined evolution of antibody escape with enhanced antagonism of human innate immunity to improve transmission and possibly reduce immune protection from severe disease.

The most recent VOC Omicron has produced five sub-lineages BA.1-BA.5[3]. To compare their replication characteristics with Delta we first used Calu-3 human airway epithelial cells (Fig. 1a). Input doses, equalised at 2000 E gene copies, gave equivalent E RNA (RT-qPCR) at 2 hours post infection (hpi) (Fig. 1b). Omicron isolates BA.1, BA.2 and BA.5 replicated similarly, lagging behind Delta initially, but largely catching up by 24 hpi (Fig. 1a). BA.4 replicated most slowly but also caught up with BA.1, BA.2 and BA.5 by 24 hpi (Fig. 1a). N positivity (Nucleocapsid [N] staining-flow cytometry) reflected E copy number when measured at 24 and 48 hpi (Fig. 1c). We

next measured the host innate immune response (RT-qPCR of interferon stimulated genes (ISGs)) in cells from Fig. 1a. Strikingly, this revealed reduced induction of Interferon-β (*IFNB*) and ISGs including inflammatory chemokine *CXCL10* and *RSAD2*, *DDX58*, *IFIT1* and *IFIT2* by BA.4 and BA.5, as compared to BA.1/BA.2 (Fig. 1d). Not all ISGs were differentially activated (*MX1* and *MX2*). However, reduced host responses to BA.4 and BA.5 were also evidenced by reduced secretion of IFNβ and CXCL10 (ELISA) (Fig.1e, f). The diminished innate immune activation by BA.4 is likely explained by slower replication in Calu-3, but BA.5 replication was similar to BA.1 and BA.2 and yet induced significantly less innate response in infected cells. The greater levels of IFNβ induced by BA.1 and BA.2 restricted their replication, because inhibition of IFN-mediated JAK/STAT signaling with Ruxolitinib rescued BA.1 and BA.2 infection in Calu-3 to a greater degree than Delta or BA.5 (Fig. 1g and S1g, l). BA.4 replication was also rescued strongly by Ruxolitinib consistent with slower replication being more sensitive to IFN inhibition (Fig. S1i-k). In infections using lower virus input doses (200 E copies) (Fig. S1a-e), we found that Delta replicated a lot better than Omicron BA.1-BA.5, and we again saw reduced innate immune activation by BA.4 and BA.5 compared to BA.1 and BA.2 (Fig. S1h). Reduced innate immune activation by BA.4 and BA.5 was also seen in a third independent experiment using 2000 E gene copy input (Fig. S1f, h).

In differentiated primary bronchial human airway epithelial cells (HAEs) Omicron BA.2, BA.4 and BA.5 sublineage isolates replicated comparably, assessed by measurement of virus released from the apical side of the cultures over time (E RNA by RT-pPCR) (Fig. 1h, i). Consistent with a previous report using a primary upper airway model[13,14] we found that Omicron isolates replicated faster than Delta by 24 hpi (Fig. 1h, i). However, while intracellular E copies were broadly similar at 72 hpi between isolates (Fig 1h, j), we consistently observed a trend towards less ISG induction by recent BA.4 and BA.5 isolates compared to parental BA.2 in HAE cells (*IFNB, CXCL10, IFIT1,*

IFIT2, DDX58 and *RSAD2*) (Fig. 1k). Blockade of IFN signalling by JAK/STAT inhibition with Ruxolitinib rescued replication of BA.2, BA.4 and BA.5 to the same degree (Fig. 1j). As expected, Ruxolitinib treatment suppressed induction of ISGs (Fig. 1k). Similar host responses and high replication levels across Omicron isolates in HAE are consistent with Omicron's epidemiological success globally. These replication experiments, particularly in Calu-3, suggested differences in innate immune antagonism between early (BA.1, BA.2) and late (BA.4, BA.5) Omicron isolates and therefore we sought to better understand the reasons underlying these different host responses.

We previously discovered that Alpha evolved enhanced innate immune evasion and this was associated with increased expression of key innate antagonists Orf6, Orf9b and N[15]. Calu-3 infection with 2000 E gene copies led to similar levels of E RNA at 48 hpi (Fig. 2a). However, immunoblots detecting viral proteins at this time point suggested that BA.5 expressed higher levels of Orf6 and N (Fig. 2b and S2a). Indeed, quantitation of two immunoblots from independent experiments supported higher levels of Orf6 for BA.4 and BA.5 and higher N levels for BA.5 (Fig. 2c, d and S2b, d). Neutralising the effect of IFN with Ruxolitinib rescued viral replication of all Omicron lineages as before (Fig. 1g and S1g, l) and enhanced expression of all viral proteins but enhancement of BA.4 and BA.5 Orf6 and N expression was still apparent (Fig. 2b, e, f and S2a, c, e, g). In contrast to Alpha[15] (Fig. S2i-k) subgenomic RNA (sgRNA) for Orf6 and N, and S and Orf3a as controls, were not particularly enhanced when measured with respect to Orf1a gRNA (Fig. 2g-j). Unlike Alpha[15] expression of innate immune antagonist Orf9b was not detected for the Omicron isolates but was readily detectable in Delta infected cells (Fig. 2k and Fig. S2h). Although Omicron subvariants encode synonymous and non-synonymous mutations in Orf6 and N they do not correlate with altered Orf6 or N expression or changes in innate immune antagonism (Fig. 1 and 2, Table S1, S2). We hypothesise that increased Orf6 translation or enhanced protein

stability, perhaps through increasing a viral Orf6 binding partner, explains enhanced Orf6 expression.

To further probe the role of Orf6 in innate immune antagonism during infection, we generated an Alpha Orf6 deletion virus by reverse genetics (Alpha ∆Orf6). Alpha ∆Orf6 replicated similarly to wild type virus in Calu-3 cells up to 24 hpi (Fig. 3a). Consistent with an important role for Orf6 in innate immune antagonism[15–17], we found increased IRF3 nuclear translocation after Alpha ∆Orf6 infection at 24 hpi (single cell quantitative immunofluorescence microscopy) (Fig. 3b). This is consistent with previous work demonstrating Orf6 over-expression in isolation directly suppresses IRF3 nuclear transport[16–18]. Concordantly, *IFNB* and *CXCL10* gene induction (Fig. 3c, d) and protein secretion (Fig. 3e, f) were enhanced in response to Alpha ∆Orf6 infection compared to WT. The small reduction in replication at 48 hpi and N and S protein expression at 24 hpi was rescued by Ruxolitinib treatment consistent with greater IFN induction after mutant virus infection (Fig.3g, h).

In HAE cells, Alpha ∆Orf6 replicated less well than WT (Fig. 3i-k). *IFNB* and *CXCL10* gene induction were similar between Alpha ∆Orf6 and WT (Fig. 3l), despite the differences in replication, consistent with increased innate immune induction by Alpha ∆Orf6 when viral RNA levels are taken into account. The deficit in Alpha ∆Orf6 replication was rescued by inhibiting IFN signaling with Ruxolitinib whereas WT replication was unaffected, consistent with the notion that IFN induction caused the reduced replication of the mutant virus (Fig. 3i). Together these data confirm Orf6 as a viral innate immune antagonist, and are consistent with a model in which, like Alpha, BA.5 enhancement of Orf6 expression contributes to the reduced innate immune response as compared to its parental BA.2 isolate.

Omicron is defined by adaptation of spike to evade antibody responses in a largely vaccinated, or pre-infected, population. Endosomal cathepsins or cell surface TMPRSS2, are required to cleave spike at the S1-S2 boundary prior to ACE2 mediated entry[19,20]. A consequence of Omicron spike adaptation is the ability to use cathepsin dependent endosomal entry routes, with reduced dependence on TMPRSS2[13,21–23]. To examine Omicron evolution of cell entry in the most recent Omicron BA.5 isolate, we examined infectivity of viruses on Calu-3, where entry is largely TMPRSS2-dependent and Camostat sensitive (Fig.4a) and HeLa over-expressing ACE2, where entry is largely cathepsin-dependent and E64d sensitive (Fig. 4b). When virus doses were equalised by E RNA copy RT-qPCR, we found that BA.5 had enhanced infectivity on HeLa-ACE2, suggesting that it is particularly well-adapted to using cathepsin-dependent endosomal entry pathways. We detected no difference in virion spike cleavage between Omicron isolates (Fig. 4c).

Finally, we examined whether Omicron lineages have adapted to replicate at lower temperature, as might be expected if they have adapted to replicate in the upper airway, where temperatures are cooler. In fact, we found that all of the Omicron isolates replicated less well in Calu-3 at 32˚C, as compared to replication at 37˚C (Fig. 4d, e). Delta replication was less sensitive to reduced temperature. We also measured innate immune responses to temperature change measuring *IFNB* and *CXCL10* mRNA induction (Fig 4f, g). We found that, as expected[24], lowering the temperature reduced the innate immune response to infection (Fig. 4f, g) and to poly:IC transfection of Calu-3 cells (Fig. 4h). This experiment reiterated that innate responses to BA.5 infection are particularly low. We also measured the effect of temperature on replication in HAE cells, again standardising dose by viral E copy RT-qPCR (Fig. 4i-l). In HAE, intracellular viral replication was less impacted by lowering the temperature from 37-32˚C than in Calu-3 (Fig. 4i).

However, apical washes from infected HAE cultures demonstrated similarly reduced virus output between Omicron isolates at 32˚C (Fig. 4j-l). Concordant with the reduced innate immune activation in Calu-3 cells at lower temperature, HAEs also expressed significantly less *IFNB* and *CXCL10* at 32˚C (Fig. 4m, n). These data suggest that Omicron may not have adapted to replicate at lower temperatures.

Innate immunity is a potent first-line defense against viral transmission[25,26] and severe COVID-19 disease has been linked with inborn errors of interferon activity and interferon neutralising autoantibodies[27–31]. Here, we provide evidence that the most recent Omicron variants BA.4 and BA.5 are better able to suppress innate immune sensing (Fig. 1) as compared to earlier Omicron variants BA.1 and BA.2. These data are consistent with ongoing adaptation of the Omicron lineage to human innate immunity, with these adaptations perhaps contributing to recent surges in COVID-19 cases and hospitalisation. Our observation of enhanced Orf6 and N expression for recent Omicron isolates is reminiscent of enhancement of Orf6, Orf9b and N expression in Alpha[15], and suggests a common pathway of adaptation to combat human innate immunity. We propose that changes outside spike have significant impact on viral transmission and disease severity and that ongoing linkage of genotype to phenotype will assist prediction of which variants will be most cause for concern as they arise.

References

1. Viana, R. *et al.* Rapid epidemic expansion of the SARS-CoV-2 Omicron variant in southern Africa. *Nature* **603**, 679–686 (2022).
2. Pulliam, J. R. C. *et al.* Increased risk of SARS-CoV-2 reinfection associated with emergence

of Omicron in South Africa. *Science* **376**, eabn4947 (2022).

3. Tegally, H. *et al.* Emergence of SARS-CoV-2 Omicron lineages BA.4 and BA.5 in South Africa. *Nat. Med.* (2022) doi:10.1038/s41591-022-01911-2.
4. Hachmann, N. P. *et al.* Neutralization escape by the SARS-CoV-2 Omicron variants BA.2.12.1 and BA.4/BA.5. *medRxiv* (2022) doi:10.1101/2022.05.16.22275151.
5. Gruell, H. *et al.* Delineating antibody escape from Omicron sublineages. *bioRxiv* 2022.04.06.487257 (2022) doi:10.1101/2022.04.06.487257.
6. Wang, Q. *et al.* Antibody evasion by SARS-CoV-2 Omicron subvariants BA.2.12.1, BA.4, and BA.5. *bioRxiv* 2022.05.26.493517 (2022) doi:10.1101/2022.05.26.493517.
7. Tuekprakhon, A. *et al.* Further antibody escape by Omicron BA.4 and BA.5 from vaccine and BA.1 serum. *bioRxiv* 2022.05.21.492554 (2022) doi:10.1101/2022.05.21.492554.
8. Willett, B. J. *et al.* Distinct antigenic properties of the SARS-CoV-2 Omicron lineages BA.4 and BA.5. *bioRxiv* 2022.05.25.493397 (2022) doi:10.1101/2022.05.25.493397.
9. Kimura, I. *et al.* Virological characteristics of the novel SARS-CoV-2 Omicron variants including BA.2.12.1, BA.4 and BA.5. *bioRxiv* 2022.05.26.493539 (2022) doi:10.1101/2022.05.26.493539.
10. Khan, K. *et al.* Omicron sub-lineages BA.4/BA.5 escape BA.1 infection elicited neutralizing immunity. *bioRxiv* (2022) doi:10.1101/2022.04.29.22274477.
11. Cao, Y. *et al.* BA.2.12.1, BA.4 and BA.5 escape antibodies elicited by Omicron infection. *Nature* (2022) doi:10.1038/s41586-022-04980-y.
12. Steel, K., Fordham, E. & Bracher, M. Coronavirus (COVID-19) infection survey, UK - office for national statistics. https://www.ons.gov.uk/peoplepopulationandcommunity/healthandsocialcare/conditionsanddiseases/bulletins/coronaviruscovid19infectionsurveypilot/1july2022 (2022).
13. Peacock, T. P. *et al.* The altered entry pathway and antigenic distance of the SARS-CoV-2 Omicron variant map to separate domains of spike protein. *BioRxiv*

doi:10.1101/2021.12.31.474653.

14. Willett, B.J. *et al*. SARS-CoV-2 Omicron is an immune escape variant with an altered cell entry pathway. *Nat. Microbiol.* doi: 10.1038/s41564-022-01143-7. Online ahead of print.
15. Thorne, L. G. *et al.* Evolution of enhanced innate immune evasion by SARS-CoV-2. *Nature* **602**, 487–495 (2022).
16. Miorin, L. *et al.* SARS-CoV-2 Orf6 hijacks Nup98 to block STAT nuclear import and antagonize interferon signaling. *Proc. Natl. Acad. Sci. U.S.A.* **117**, 28344–28354 (2020).
17. Lei, X. *et al.* Activation and evasion of type I interferon responses by SARS-CoV-2. *Nat. Commun.* **11**, 3810 (2020).
18. Addetia, A. *et al.* SARS-CoV-2 ORF6 Disrupts Bidirectional Nucleocytoplasmic Transport through Interactions with Rae1 and Nup98. *MBio* **12**, (2021).
19. Hoffmann, M., Kleine-Weber, H. & Pöhlmann, S. A Multibasic Cleavage Site in the Spike Protein of SARS-CoV-2 Is Essential for Infection of Human Lung Cells. *Mol. Cell* **78**, 779–784.e5 (2020).
20. Hoffmann, M. *et al.* SARS-CoV-2 Cell Entry Depends on ACE2 and TMPRSS2 and Is Blocked by a Clinically Proven Protease Inhibitor. *Cell* **181**, 271–280.e8 (2020).
21. Meng, B. *et al.* Altered TMPRSS2 usage by SARS-CoV-2 Omicron impacts infectivity and fusogenicity. *Nature* **603**, 706–714 (2022).
22. Willett, B. J. *et al.* The hyper-transmissible SARS-CoV-2 Omicron variant exhibits significant antigenic change, vaccine escape and a switch in cell entry mechanism. *medRxiv* doi:10.1101/2022.01.03.21268111. (2022)
23. Mesner, D. *et al.* SARS-CoV-2 Spike evolution influences GBP and IFITM sensitivity. *bioRxiv* 2022.03.07.481785 (2022) doi:10.1101/2022.03.07.481785.
24. Foxman, E. F. *et al.* Temperature-dependent innate defense against the common cold virus limits viral replication at warm temperature in mouse airway cells. *Proc. Natl. Acad. Sci. U.S.A.* **112**, 827–832 (2015).

25. Sandler, N. G. *et al.* Type I interferon responses in rhesus macaques prevent SIV infection and slow disease progression. *Nature* **511**, 601–605 (2014).
26. Sumner, R. P. *et al.* Are Evolution and the Intracellular Innate Immune System Key Determinants in HIV Transmission? *Front. Immunol.* **8**, 1246 (2017).
27. Zhang, Q. *et al.* Inborn errors of type I IFN immunity in patients with life-threatening COVID-19. *Science* **370**, (2020).
28. Bastard, P. *et al.* Autoantibodies against type I IFNs in patients with life-threatening COVID-19. *Science* **370**, (2020).
29. Pairo-Castineira, E. *et al.* Genetic mechanisms of critical illness in COVID-19. *Nature* **591**, 92–98 (2021).
30. Zhang, Q., Bastard, P., COVID Human Genetic Effort, Cobat, A. & Casanova, J.-L. Human genetic and immunological determinants of critical COVID-19 pneumonia. *Nature* **603**, 587–598 (2022).
31. Wickenhagen, A. *et al.* A prenylated dsRNA sensor protects against severe COVID-19. *Science* **374**, eabj3624 (2021).
32. Rogers, T. F. *et al.* Isolation of potent SARS-CoV-2 neutralizing antibodies and protection from disease in a small animal model. *Science* **369**, 956–963 (2020).
33. Thorne, L. G. *et al.* SARS-CoV-2 sensing by RIG-I and MDA5 links epithelial infection to macrophage inflammation. *EMBO J.* **40**, e107826 (2021).
34. Zhou, J. *et al.* Mutations that adapt SARS-CoV-2 to mink or ferret do not increase fitness in the human airway. *Cell Rep.* **38**, 110344 (2022).
35. Thi Nhu Thao, T. *et al.* Rapid reconstruction of SARS-CoV-2 using a synthetic genomics platform. *Nature* **582**, 561–565 (2020).
36. Rihn, S. J. *et al.* A plasmid DNA-launched SARS-CoV-2 reverse genetics system and coronavirus toolkit for COVID-19 research. *PLoS Biol.* **19**, e3001091 (2021).
37. da Silva Filipe, A. *et al.* Genomic epidemiology reveals multiple introductions of SARS-CoV-

2 from mainland Europe into Scotland. *Nat Microbiol* **6**, 112–122 (2021).

38. Parker, M. D. *et al.* Altered Subgenomic RNA Expression in SARS-CoV-2 B.1.1.7 Infections. *bioRxiv* 2021.03.02.433156 (2021) doi:10.1101/2021.03.02.433156.

39. Meredith, L. W. *et al.* Rapid implementation of SARS-CoV-2 sequencing to investigate cases of health-care associated COVID-19: a prospective genomic surveillance study. *Lancet Infect. Dis.* **20**, 1263–1272 (2020).

40. Schindelin, J. *et al.* Fiji: an open-source platform for biological-image analysis. *Nat. Methods* **9**, 676–682 (2012).

Figure legends

Fig 1. BA.5 displays enhanced innate immune antagonism during infection of airway epithelial cells.

(a-f) Calu-3 infection with 2000 E copies/cell of Delta (orange; O), BA.1 (blue; O), BA.2 (blue; Δ), BA.4 (purple; O) and BA.5 (purple; Δ), n=3. (**a**) Viral replication over time measured by RT-qPCR for intracellular E copies. (**b**) Viral E copies at 2 hpi in cells from (a). (**c**) Infection levels measured by nucleocapsid expression (% N+ by flow cytometry). (**d**) Expression *IFNB*, *CXCL10*, *IFIT1, IFIT2, RSAD2, MX1, MX2* and *DDX58* in infected cells over time. (**e**) IFNβ and (**f**) CXCL10 secretion from infected Calu-3 cells measured by ELISA at 48 hpi. (**g**) Viral replication of indicated variants in Calu-3 cells infected at 200 E copies/cell in the presence or absence of 5μM Ruxolitinib at 48 hpi. (h-k) Primary bronchial human airway epithelial cells (HAEs) were infected with 1500 E copies/cell of the indicated variants, n=3. Viral replication was measured by (**h**) intracellular E copies at 72 hpi and (**i**) viral release into apical washes over time. (**j**) Intracellular viral E copies in HAEs in the presence or absence of Ruxolitinib at 72hpi. (**k**) Expression of *IFNB*, *CXCL10, IFIT1*, *IFIT2*, *DDX58* and *RSAD2* in cells from (j). Fold changes are normalised to mock at (d) 2 hpi or

(k) 72 hpi. For statistical comparisons at each time point in (a-e), One-way ANOVA with Dunnett's post-test was used to compare BA.2 with other variants. For (a, d) colours indicate comparator (Delta, yellow; BA.1, blue; BA.4, purple; BA.5, pink). For (g-k), pairwise comparisons were performed using a Student's t-Test as indicated. Mean+/-SEM or individual datapoints are shown. hpi, hours post infection. *, $p<0.05$; **, $p<0.01$; ***, $p<0.001$; n.s., not significant or exact p-value given (k).

Fig 2. BA.5 efficiently expresses SARS-CoV-2 innate antagonists during airway epithelial cell infection.

Calu-3 cells were infected with 2000 E copies/cell of the indicated variants. (**a**) Viral replication at 48hpi. (**b**) Representative western blot of Orf6, N, spike/S2 and β-Actin at 48 hpi in infected cells +/- 5μM Ruxolitinib. Non-specific bands detected by polyclonal anti-spike primary antibody are indicated (see Fig. S2a for Mock). (c-f) Densitometry quantification of (**c**) Orf6 and (**d**) N in cells untreated or (**e**) Orf6 and (**f**) N in Ruxolitinib-treated cells from blots in (a and Fig. S2a) normalised to spike+S2 over BA.2, n=2. (g-h) sgRNA expression of (**g**) Orf6, (**h**) N, (**i**) spike and (**j**) Orf3a normalised to Orf1a genomic RNA in Calu-3 cells at 48 hpi, n=9. (**k**) Western blot of Orf9b, Orf6, N and β-Actin at 48 hpi in infected cells +5μM Ruxolitinib. For (g-h) one-way ANOVA with Dunnett's post-test was used to compare BA.2 with other variants. Mean+/-SEM or individual datapoints are shown. hpi, hours post infection. sgRNA, subgenomic RNA. *, $p<0.05$; ***, $p<0.001$; n.s., not significant.

Fig. 3: Orf6 expression is a major determinant of enhanced innate immune antagonism by emerging VOCs.

(a) Replication of reverse genetic (RG) viruses Alpha WT and ΔOrf6 in Calu-3 cells infected with 2000 E copies/cell over time, n=3. (**b**) Quantification of IRF3 translocation detected by single-cell

fluorescence microscopy over time. Data from 1500 cells/condition are shown. (**c**) *IFNB* and (**d**) *CXCL10* expression in cells from (a) over time, n=3. (**e**) IFNβ and (**f**) CXCL10 secretion from infected Calu-3 cells measured at 48 hpi, n=2. (**g**) Viral replication in the presence or absence of 5μM Ruxolitinib at 48 hpi in cells from (a). (**h**) Western blot of RG virus infections in Calu-3 cells at 24 hpi for spike, N, Orf6 and β-Actin +/- Ruxolitinib. (i-l) Primary bronchial human airway epithelial cells (HAEs) were infected with 1500 E copies/cell of the indicated variants in the presence or absence of 5 μM Ruxolitinib, (n=3). Viral replication was measured by (**i**) intracellular E copies at 72 hpi and (**j, k**) viral release into apical washes over time. (**l**) *IFNB* and *CXCL10* expression in cells from (i), Fold changes are normalised to mock at 2 hpi. For statistical comparisons at each time point in (a, c-g, i-l). One-way ANOVA with Dunnett's post-test was used to compare groups as indicated. In (b), a Kruskal-Wallis test was used to compare groups at 24 hpi. Mean+/-SEM or individual datapoints are shown. hpi, hours post infection. $p<0.05$; **, $p<0.01$; ***, $p<0.001$; n.s., not significant.

Fig 4. Entry and replication characteristics of Omicron lineage BA.5.

(**a**) Calu-3 and (**b**) Hela-ACE2 cells were infected with 1000 E copies/cell of the indicated variants in the presence of DMSO (-), 25 μM E64d or 25 μM Camostat. Infection levels were measured at 24 hpi by nucleocapsid expression (% N+ by flow cytometry), n=3. (**c**) Representative western blot of spike and N in purified SARS-CoV-2 virions, n=2. (d-g) Calu-3 cells were infected with 2000 E copies/cell at 37ºC or 32ºC, n=3. (**d**) Viral replication by RT-qPCR and (**e**) infection levels by flow cytometry at 24 hpi. (**f**) *IFNB* and (**g**) *CXCL10* expression in cells from (d). (**h**) *IFNB* and *CXCL10* expression in response to poly:IC transfection in Calu-3 cells at 24h of stimulation, n=2. (i-n) Primary bronchial human airway epithelial cells (HAEs) were infected with 1500 E copies/cell of the indicated variants at 37ºC or 32ºC, n=3. Viral replication was measured by (**i**) intracellular E copies at 72 hpi and viral release of (**j**) BA.2, (**k**) BA.4 and (**l**) BA.5 into apical washes over time. Relative expression of (**m**) *IFNB* and (**n**) *CXCL10* normalised to *GAPDH* in cells from (i). Fold

changes are normalised to mock. Pairwise comparisons were performed using a Student's t-Test as indicated. Mean+/-SEM or individual datapoints are shown. hpi, hours post infection. *, p<0.05 ; **, p<0.01; ***, p<0.001; n.s., not significant or exact p-value given (k).

Fig S1. BA.5 displays enhanced innate immune antagonism during infection of airway epithelial cells.

(a-e) Calu-3 infection with 200 E copies/cell of Delta (orange; O), BA.1 (blue; O), BA.2 (blue; Δ), BA.4 (purple; O) and BA.5 (purple; Δ), n=3. (**a**) Viral replication over time measured by RT-qPCR for intracellular E copies. (**b**) Viral E copies at 2hpi in cells from (a). (**c**) Infections levels measured by nucleocapsid expression (% N+ by flow cytometry). Expression (**d**) *IFNB* or (**e**) *CXCL10* and *IFIT1* in infected cells at 24 hpi, n=3. (f-h) Calu-3 infection with 2000 E copies/cell of indicated variants, n=3. (**f**) Viral replication over time, n=3. (**g**) Viral replication of indicated variants in Calu-3 cells in the presence or absence of 5μM Ruxolitinib at 48 hpi, n=3. (**h**) *IFNB*, *CXCL10*, *IFIT1, IFIT2, RSAD2, MX1, MX2* and *DDX58* expression at 24 hpi, n=3. (i-k) IFNβ-sensitivity of indicated variants during Calu-3 cell infection at 2000 E copies/cell. (**i**) Infection levels measured by % N+ at 24 hpi at the indicated concentrations of IFNβ, n=6. (**j**) Infection levels in cells from (i) at 0 ng/ml IFNβ, n=6. (**k**) Infection levels from (i) normalised to 0 ng/ml IFNβ for each variant, n=6. (**l**) Fluorescence microscopy of Calu-3 cells infected at 2000 E copies/cell at 48 hpi in the presence or absence of 5μM Ruxolitinib. Percentage infection quantified by dsRNA-positive cells is indicated per condition. Representative images shown. Scale bar, 50 μm. (d, e, h). Fold changes are normalised to mock at 24 hpi. For statistical comparisons at each time point in (a-c, f, i-k), One-way ANOVA with Dunnett's post-test was used to compare BA.2 with other variants. For (a, f) colours indicate comparator (Delta, yellow; BA.1, blue; BA.4, purple; BA.5, pink). For (d, e, g, h), pairwise comparisons were performed using a Student's t-Test as indicated. Mean+/-SEM or individual datapoints are shown. hpi, hours post infection. *, p<0.05 ; **, p<0.01; ***, p<0.001; n.s., not significant.

Fig S2. BA.5 efficiently expresses SARS-CoV-2 innate antagonists during airway epithelial cell infection.

(**a**) Western blot of Orf6, N, spike/S2 and β-Actin at 48 hpi in infected Calu-3 cells +/- 5μM Ruxolitinib. Non-specific bands detected by polyclonal anti-spike primary antibody are indicated. Densitometry quantification of western blots in (a) and Fig. 2 a of (**b, c**) Orf6, (**d**, **e**) N and (**f**, **g**) spike+S2 normalised to β-Actin over BA.2 at 48 hpi, n=2. (**h**) Western blot of Orf9b, Orf6, spike and β-Actin at 24 hpi in infected cells. (**i**) Viral replication by RT-qPCR at 24 hpi, n=3. (**j**) Orf6 and (**k**) N sgRNA expression in cells from (i), n=3. For (i, j, k). One-way ANOVA with Dunnett's post-test was used to compare BA.2 with other variants. Mean+/-SEM or individual datapoints are shown. hpi, hours post infection. sgRNA, subgenomic RNA. *, $p<0.05$; ***, $p<0.001$; n.s., not significant.

Table S1 Orf6 mutations detected in the Omicron sub-lineages

Table S2 Nucleocapsid (N) mutations detected in the Omicron sub-lineages

Methods

Cell culture

Calu-3 cells were purchased from AddexBio (C0016001), Caco-2 cells were a kind gift from Dalan Bailey (Pirbright Institute) and Hela-ACE2 cells were a gift from James E Voss[32]. Cell lines were cultured in Dulbecco's modified Eagle Medium (DMEM) supplemented with 10% heat-inactivated FBS (Labtech) and 100U/ml penicillin/streptomycin. Cells were passaged at 80-90% confluence. For infections, Calu-3 and Caco-2 cells were seeded at $2x10^5$ cells/ml and Hela-ACE2 cells at

369 1x10^5 cells/ml and grown to 60-80% confluence for experiments[15,33]. Primary normal (healthy)
370 bronchial epithelial (NHBE-A) cells were cultured for five to seven passages and differentiated at
371 an air-liquid interface as previously described[15]. After 21-24 days of differentiation, cells were
372 used in infection experiments.

373 **Viruses**

374 SARS-CoV-2 lineages Alpha (B.1.1.7)[15], Delta (B.1.617.2)[13] and Omicron (lineage
375 B.1.1.529.1/BA.1 and lineage B.1.1.529.2/BA.2) isolates were a gift from Wendy Barclay (Imperial
376 College London, UK). Omicron BA.4 (lineage B.1.1.529.4) and BA.5 (lineage B.1.1.529.5) were
377 a gift from Alex Sigal and Khadija Khan (Africa Health Research Institute, Durban, South
378 Africa)[3,10]. Alpha Orf6 deletion virus (Alpha ΔOrf6) was achieved by mutation of the first two
379 methionines: M1L (A27216T) and M19L (A27200T). Reverse genetics derived viruses were
380 generated essentially as previously described[34,35] . In brief, to generate the WT SARS-CoV-2
381 Alpha variant, a set of overlapping viral genomic cDNA fragments were chemically synthesised
382 (GENEWIZ, Germany). The cDNA fragment representing the 5' terminus of the viral genome
383 contained the bacteriophage T7 RNA polymerase promoter and the fragment representing the 3'
384 terminus contained the T7 RNA polymerase termination sequences. These fragments were then
385 assembled into full-length Alpha cDNA genome using the Transformation-Associated
386 Recombination (TAR) in yeast method[34]. To generate the Alpha virus carrying the ATG codon
387 changes (M1L and M19L) in its Orf6 gene, the relevant cDNA fragments carrying the desired
388 mutations were chemically synthesized (Thermofisher, UK) and the mutant viral genome was
389 assembled using TAR in yeast as described above. The assembled WT and Orf6 null mutant
390 genomes were used as templates to *in vitro* transcribe viral genomic RNA which was then
391 transfected into BHK-hACE2-N cells stably expressing the SARS-CoV-2 N and the human ACE2
392 gene for virus rescue[36]. The rescued viruses were passaged once (P1 stock) in Vero.E6 cells and
393 their full genomes sequenced using Oxford Nanopore as previously described[37]. All viruses were

propagated by infecting Caco-2 cells in DMEM culture medium supplemented with 1% FBS and 100U/ml penicillin/streptomycin at 37 °C as previously described[15,33]. Virus was collected at 72 hpi and clarified by centrifugation at 2,100xg for 15 min at 4°C to remove any cellular debris. Virus stocks were aliquoted and stored at −80 °C. Virus stocks were quantified by extracting RNA from 100 µl of supernatant with 1 µg/ml carrier RNA using Qiagen RNeasy clean-up RNA protocol, before measuring viral E RNA copies per ml by RT-qPCR[15,33].

Virus culture and infection

For infections, inoculum was calculated using E copies per cell quantified by RT-qPCR. Cells were inoculated with indicated variants for 2 h at 37°C, subsequently washed with PBS and fresh DMEM culture medium supplemented with 1% FBS and 100U/ml penicillin/streptomycin was added. At the indicated time points, cells were collected for analysis. For primary HAE infections, virus was added to the apical side for 2-3 h at 37°C. Supernatant was then removed and cells were washed twice with PBS. All liquid was removed from the apical side and basal medium was replaced with fresh Pneumacult ALI medium for the duration of the experiment. Virus release was measured at the indicated time points by extracting viral RNA from apical PBS washes. For IFN-sensitivity assays, cells were pre-treated with indicated concentrations or recombinant human IFNβ (Peprotech) for 18h before infection. Cytokines were maintained throughout the experiment. For inhibition assays, cells were pre-treated with 5 µM Ruxolitinib (Cambridge Bioscience), 25 µM camostat (Apexbio), 25 µM E64d (Focus Biomolecules) or DMSO control for 2-3 h before SARS-CoV-2 infection. Inhibitors were maintained throughout the infection.

RT-qPCR of host and viral gene expression in infected cells

Infected cells were lysed in RLT (Qiagen) supplemented with 0.1% beta-mercaptoethanol (Sigma). RNA extractions were performed according to the manufacturer's instructions using RNeasy Micro Kits (Qiagen) including on-column DNAse I treatment (Qiagen). cDNA was

synthesized using SuperScript IV (Thermo) with random hexamer primers (Thermo). RT-qPCR was performed using Fast SYBR Green Master Mix (Thermo) for host gene expression and subgenomic RNA expression or TaqMan Master mix (Thermo Fisher Scientific) for viral RNA quantification, and reactions were performed on the QuantStudio 5 Real-Time PCR systems (Thermo Fisher Scientific). Viral E RNA copies were determined as described previously[15,33]. Viral subgenomic RNAs were detected using the same forward primer against the leader sequence paired with a sgRNA specific reverse primer[15,38,39]. Using the 2−ΔΔCt method, sgRNA levels were normalised to GAPDH to account for differences in RNA loading and then normalised to the level of Orf1a gRNA quantified in the same way for each variant to account for differences in the level of infection. Host gene expression was determined using the 2−ΔΔCt method and normalised to GAPDH expression. The following probes and primers were used:

GAPDH fw: 5'-ACATCGCTCAGACACCATG-3', rv: 5'-TGTAGTTGAGGTCAATGAAGGG-3'; *IFNB* fw: 5'-GCTTGGATTCCTACAAAGAAGCA-3', rv: 5'-ATAGATGGTCAATGCGGCGTC-3'; *CXCL10* fw: 5'-TGGCATTCAAGGAGTACCTC-3', rv: 5'-TTGTAGCAATGATCTCAACACG-3'; *IFIT1* fw: 5'-CCTCCTTGGGTTCGTCTACA-3', rv: 5'-GGCTGATATCTGGGTGCCTA-3'; *IFIT2* fw: 5′-CAGCTGAGAATTGCACTGCAA-3′, rv: 5′-CGTAGGCTGCTCTCCAAGGA-3′; *MX1* fw: 5′-ATCCTGGGATTTTGGGGCTT-3′, rv: 5′-CCGCTTGTCGCTGGTGTCG-3′; *MX2* fw: 5'-CAGCCACCACCAGGAAAC-3', rv 5'-TTCTGCTCGTACTGGCTGTACAG-3', *RSAD2* fw: 5′-CTGTCCGCTGGAAAGTG-3′, rv: 5′-GCTTCTTCTACACCAACATCC-3′; *DDX58* fw: 5'-CTGGACCCTACCTACATCCTG-3', rv: 5'-GGCATCCAAAAAGCCACGG-3'. SARS-CoV-2 E Sarbeco fw: 5′-ACAGGTACGTTAATAGTTAATAGCGT-3′; SARS-CoV-2 E Sarbeco Probe1: 5′-FAM-ACACTAGCCATCCTTACTGCGCTTCG-TAMRA-3′; SARS-CoV-2 E Sarbeco rv: 5′-ATATTGCAGCAGTACGCACACA-3′; 5′ Leader fw: 5'-ACCAACCAACTTTCGATCTCTTGT-3'; Orf1a rv: 5'-CCTCCACGGAGTCTCCAAAG-3'; Orf6 rv:GAGGTTTATGATGTAATCAAGATTC; N

rv: 5'-CCAGTTGAATCTGAGGGTCCAC-3'; Orf3a rv: 5'-GCAGTAGCGCGAACAAAAT-3'. S rv: 5'-GTCAGGGTAATAAACACCACGTG-3'.

Flow cytometry

Adherent cells were trypsinised and fixed in 4% formaldehyde prior to intracellular staining for SARS-CoV-2 nucleocapsid (N) protein. For N detection, cells were permeabilised for 15 min with Intracellular Staining Perm Wash Buffer (BioLegend) and subsequently incubated with 1µg/ml CR3009 SARS-CoV-2 cross-reactive antibody (a gift from Laura McCoy) for 30 min at room temperature. Primary antibodies were detected by incubation with secondary Alexa Fluor 488-Donkey-anti-Human IgG (Jackson Labs). All samples were acquired on a BD Fortessa X20 or LSR II using BD FACSDiva software. Data was analysed using FlowJo v10 (Tree Star).

Cytokine secretion

Secreted mediators were detected in cell culture supernatants by ELISA. IFNβ and CXCL10 were measured using Human IFN-beta Quantikine ELISA Kit or Human CXCL10/IP-10 DuoSet ELISA reagents (biotechne R&D systems) according to the manufacturer's instructions.

Western blotting

For detection of N, Orf6, Orf9b, spike, MX1, IFIT1 and β-actin expression, whole-cell protein lysates were extracted with RIPA buffer, and then separated by SDS–PAGE, transferred onto nitrocellulose and blocked in PBS with 0.05% Tween 20 and 5% skimmed milk. Membranes were probed with rabbit-anti-IFIT1 (CST, #14769, clone D2X9Z), rabbit-anti-MX1 (CST, #37849, clone D3W7I) rabbit-anti-SARS spike (Invitrogen, PA1-411-1165), rabbit-anti-Orf6 (Abnova, PAB31757), rabbit-anti-Orf9b (ProSci, 9191), Cr3009 SARS-CoV cross-reactive human-anti-N antibody (a gift from Laura McCoy, UCL) and rabbit-anti-beta-actin (SIGMA), followed by IRDye 800CW or 680RD secondary antibodies (Abcam, goat anti-rabbit, goat anti-mouse or goat anti-

human). Blots were imaged using an Odyssey Infrared Imager (LI-COR Biosciences) and analysed with Image Studio Lite software. For virion blots, live virus normalised by equal total E copies was purified across a 25% sucrose cushion and concentrated by centrifugation (2h 16500xg, 4^0C).

Immunofluorescence staining and image analysis

Infected cells were fixed using 4% PFA/formaldehyde for 1 h at room temperature and subsequently washed with PBS. A blocking step was carried out for 35h at room temperature with 10% goat serum/1%BSA/0.001 Triton-TX100 in PBS. dsRNA and Nucleocapsid detection was performed by primary incubation with rabbit-anti-IRF3 antibody (sc-33641, Santa Cruz), mouse-anti-dsRNA (MABE1134, Millipore) and Cr3009 SARS-CoV cross-reactive human-anti-N antibodies for 18 h and washed thoroughly in PBS. Primary antibodies detection occurred using secondary anti-rabbit-AlexaFluor-488. anti-mouse-AlexaFluor-568 and anti-human-Alexa647 conjugates (Jackson ImmunoResearch) for 1 h. All cells were labeled with Hoechst33342 (H3570, Thermo Fisher). Images were acquired using the WiScan® Hermes 7-Colour High-Content Imaging System (IDEA Bio-Medical, Rehovot, Israel) at magnification 10X/0.4NA. Four channel automated acquisition was carried out sequentially. Images were acquired across a well area density resulting in 31 FOV/well and ~20,000 cells. Images were pre-processed by applying a batch rolling ball background correction in FIJI ImageJ software package[40] prior to quantification. IRF3 translocation analysis was carried out using the Athena Image analysis software (IDEA Bio-Medical, Rehovot, Israel) and data post-processed in Python. Infected cell populations were determined by thresholding of populations with greater than 2 segmented dsRNA punctae.

Statistical analysis

Statistical analysis was performed using GraphPad Prism9 and details of statistical test used are indicated. Data shows mean +/- SEM with significant differences or exact p-values indicated in the figures. Significance levels were defined as follows: *, $p < 0.05$; **, $p < 0.01$ and ***, $p < 0.001$.

Data availability

All data generated or analysed during this study are included in this manuscript (and its supplementary information files). No new algorithms were developed for this project.

Acknowledgements

This work was funded by Wellcome Investigator Awards 223065 to C.J. and 220863 to G.J.T. G.J.T. and C.J. were also funded by MRC/UKRI G2P-UK National Virology consortium (MR/W005611/1) and the UCL COVID-19 fund. R.R is supported by a Marie Skłodowska-Curie Individual Fellowships no. 896014. P.B received funding from the European Research Council (ERC-Stg no. 639429), the Rosetrees Trust (M362-F1; M553), the NIHR GOSH BRC and the CF Trust (SRC006; SRC020). M.V.X.W. is supported by the NIHR Biomedical Research Centre at UCLH and IDEA Bio-Medical. The work at the CVR was funded by G2P-UK National Virology Consortium funded by the MRC (MR/W005611/1) and MRC grants (MC_UU12014/2) and the Wellcome Trust (206369/Z/17/Z). We are grateful to Wendy Barclay (Imperial College London, UK), and Alex Sigal and Khadija Khan (AHRI, South Africa) for provision of virus isolates and Dalan Bailey, Laura McCoy and James Voss for reagents. For the purpose of Open Access, the authors have applied a CC BY public copyright licence to any Author Accepted Manuscript version arising from this submission.

Author contributions

Conceptualisation: A-K.R., L.G.T., G.J.T. and C.J.

Designed experiments: A-K.R, L.G.T. V.C., W.F., G.d.L., G.J.T. and C.J.

Performed experiments: A-K.R, L.G.T., M.X.V.W., D.M., G.D., N.B., V.C., W.F., and G.d.L

Analysed data: A-K.R., L.G.T., M.X.V.W., G.J.T. and C.J.

Generated and provided reagents: R.R. W.F., G.de L., V.M.C., P.B., M.P. and A.H.P.

Manuscript preparation and editing: A-K.R, L.G.T., D.M., A.H.P., M.P., G.J.T. and C.J.

Coordination and supervision: P.B., M.P., A.H.P., G.J.T. and C.J.

Competing interests

The authors declare that they have no competing interests.

Correspondence and request for materials should be addressed to Ann-Kathrin Reuschl, Clare Jolly or Greg J. Towers.

Figure 1

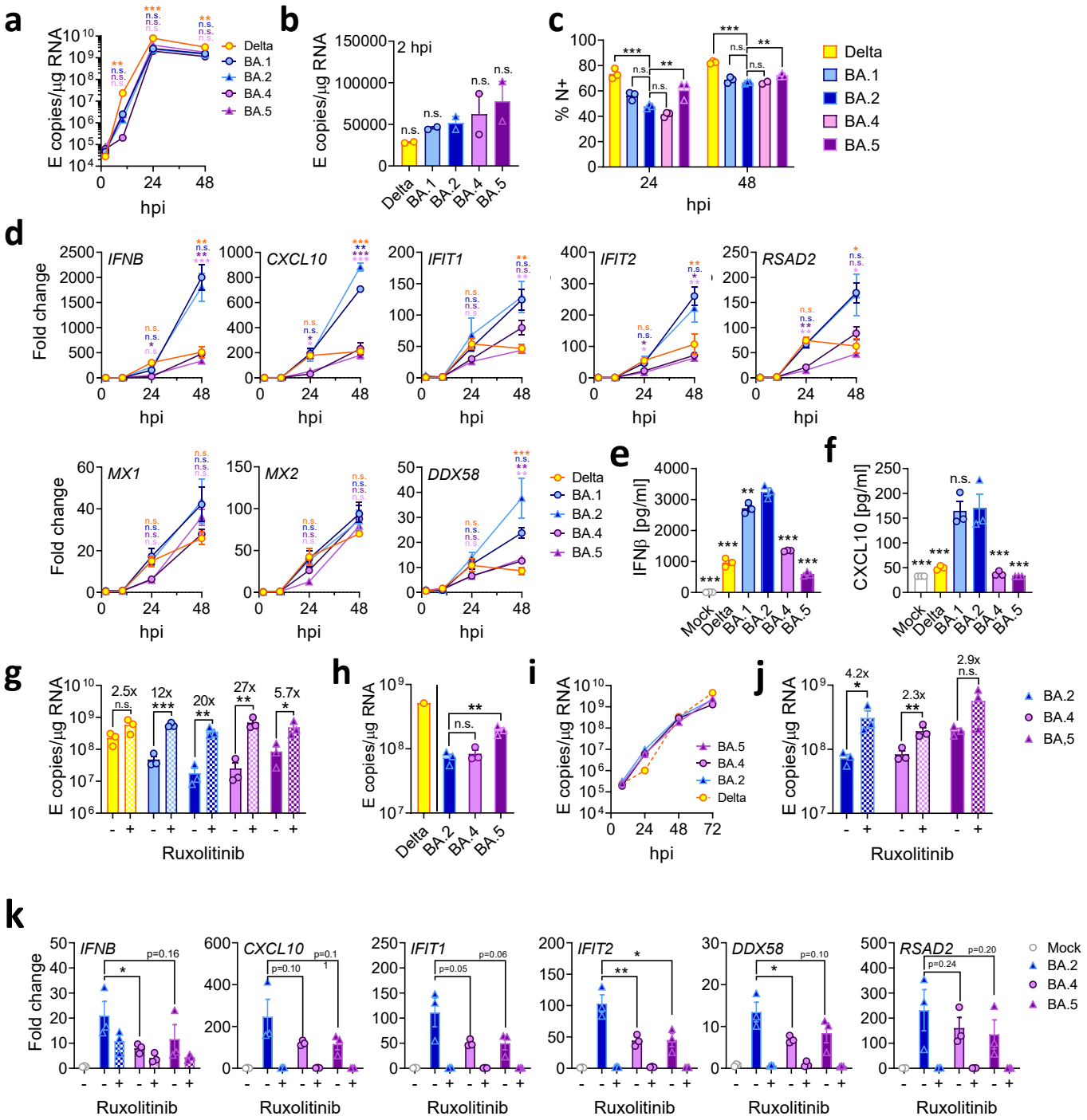

Fig 1. BA.5 displays enhanced innate immune antagonism during infection of airway epithelial cells.
(a-f) Calu-3 infection with 2000 E copies/cell of Delta (orange; O), BA.1 (blue; O), BA.2 (blue; Δ), BA.4 (purple; O) and BA.5 (purple; Δ), n=3. (**a**) Viral replication over time measured by RT-qPCR for intracellular E copies. (**b**) Viral E copies at 2 hpi in cells from (a). (**c**) Infection levels measured by nucleocapsid expression (% N+ by flow cytometry). (**d**) Expression *IFNB*, *CXCL10*, *IFIT1, IFIT2, RSAD2, MX1, MX2* and *DDX58* in infected cells over time. (**e**) IFNβ and (**f**) CXCL10 secretion from infected Calu-3 cells measured by ELISA at 48 hpi. (**g**) Viral replication of indicated variants in Calu-3 cells infected at 200 E copies/cell in the presence or absence of 5µM Ruxolitinib at 48 hpi. (h-k) Primary bronchial human airway epithelial cells (HAEs) were infected with 1500 E copies/cell of the indicated variants, n=3. Viral replication was measured by (**h**) intracellular E copies at 72 hpi and (**i**) viral release into apical washes over time. (**j**) Intracellular viral E copies in HAEs in the presence or absence of Ruxolitinib at 72hpi. (**k**) Expression of *IFNB*, *CXCL10, IFIT1*, *IFIT2*, *DDX58* and *RSAD2* in cells from (j). Fold changes are normalised to mock at (d) 2 hpi or (k) 72 hpi. For statistical comparisons at each time point in (a-e), One-way ANOVA with Dunnett's post-test was used to compare BA.2 with other variants. For (a, d) colours indicate comparator (Delta, yellow; BA.1, blue; BA.4, purple; BA.5, pink). For (g-k), pairwise comparisons were performed using a Student's t-Test as indicated. Mean+/-SEM or individual datapoints are shown. hpi, hours post infection. *, p<0.05 ; **, p<0.01; ***, p<0.001; n.s., not significant or exact p-value given (k).

Figure 2

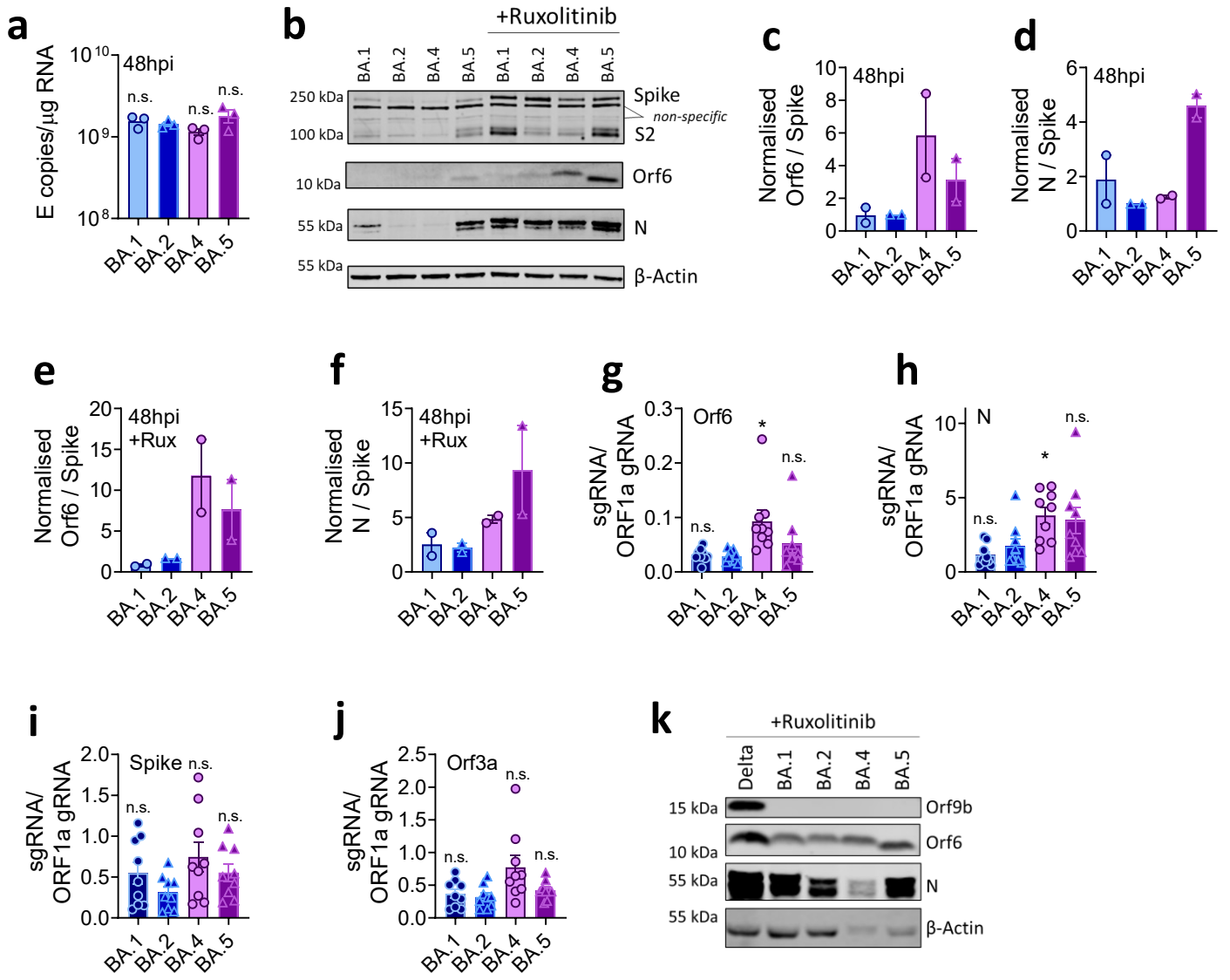

Fig 2. BA.5 efficiently expresses SARS-CoV-2 innate antagonists during airway epithelial cell infection.
Calu-3 cells were infected with 2000 E copies/cell of the indicated variants. (**a**) Viral replication at 48hpi. (**b**) Representative western blot of Orf6, N, spike/S2 and β-Actin at 48 hpi in infected cells +/- 5µM Ruxolitinib. Non-specific bands detected by polyclonal anti-spike primary antibody are indicated (see Fig. S2a for Mock). (c-f) Densitometry quantification of (**c**) Orf6 and (**d**) N in cells untreated or (**e**) Orf6 and (**f**) N in Ruxolitinib-treated cells from blots in (a and Fig. S2a) normalised to spike+S2 over BA.2, n=2. (g-h) sgRNA expression of (**g**) Orf6, (**h**) N, (**i**) spike and (**j**) Orf3a normalised to Orf1a genomic RNA in Calu-3 cells at 48 hpi, n=9. (**k**) Western blot of Orf9b, Orf6, N and β-Actin at 48 hpi in infected cells +5µM Ruxolitinib. For (g-h) one-way ANOVA with Dunnett's post-test was used to compare BA.2 with other variants. Mean+/-SEM or individual datapoints are shown. hpi, hours post infection. sgRNA, subgenomic RNA. *, $p<0.05$; ***, $p<0.001$; n.s., not significant.

Figure 3

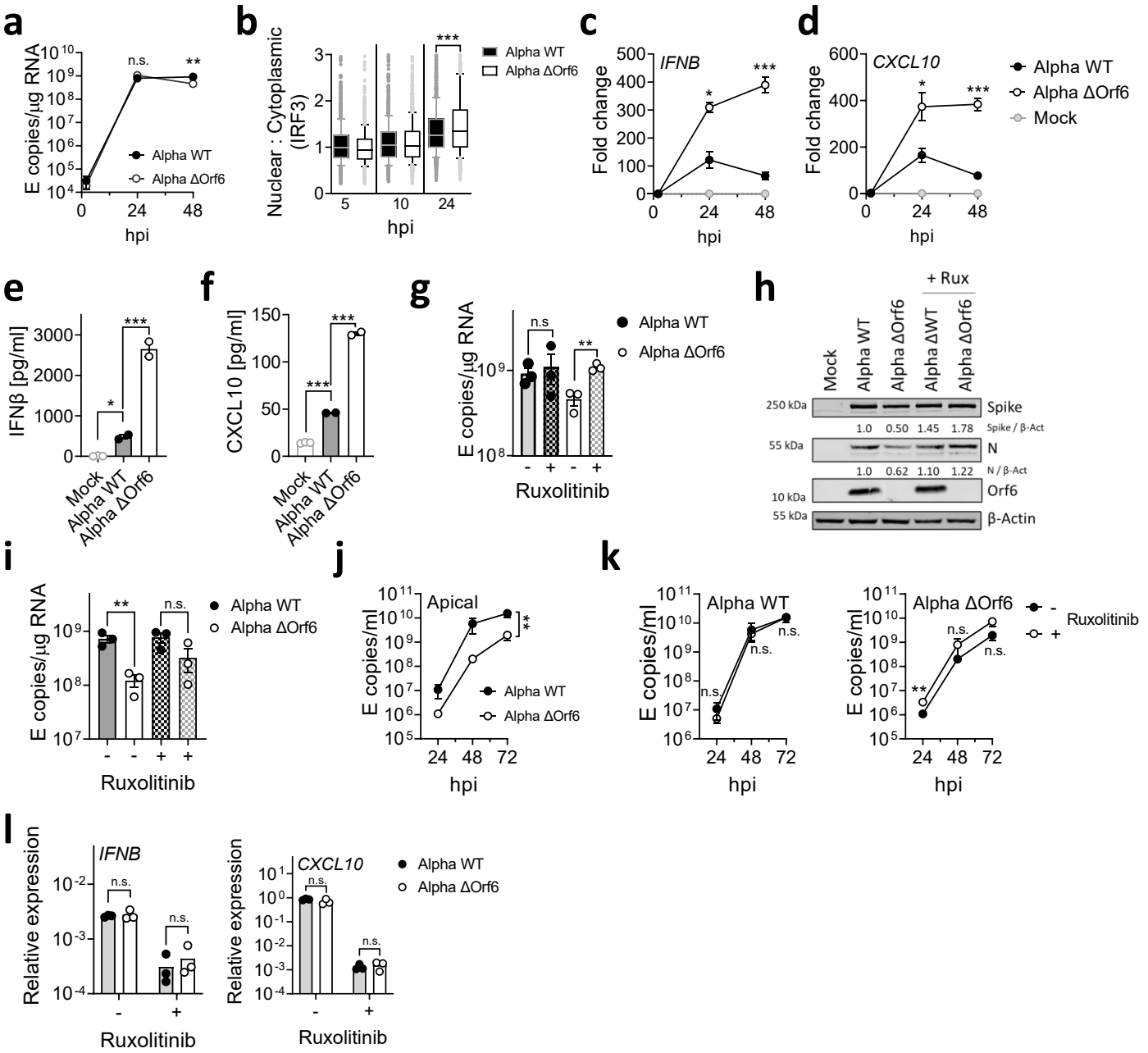

Fig. 3: Orf6 expression is a major determinant of enhanced innate immune antagonism by emerging VOCs.
(**a**) Replication of reverse genetic (RG) viruses Alpha WT and ΔOrf6 in Calu-3 cells infected with 2000 E copies/cell over time, n=3. (**b**) Quantification of IRF3 translocation detected by single-cell fluorescence microscopy over time. Data from 1500 cells/condition are shown. (**c**) *IFNB* and (**d**) *CXCL10* expression in cells from (a) over time, n=3. (**e**) IFNβ and (**f**) CXCL10 secretion from infected Calu-3 cells measured at 48 hpi, n=2. (**g**) Viral replication in the presence or absence of 5µM Ruxolitinib at 48 hpi in cells from (a). (**h**) Western blot of RG virus infections in Calu-3 cells at 24 hpi for spike, N, Orf6 and β-Actin +/- Ruxolitinib. (i-l) Primary bronchial human airway epithelial cells (HAEs) were infected with 1500 E copies/cell of the indicated variants in the presence or absence of 5 µM Ruxolitinib, (n=3). Viral replication was measured by (**i**) intracellular E copies at 72 hpi and (**j, k**) viral release into apical washes over time. (**l**) *IFNB* and *CXCL10* expression in cells from (i), Fold changes are normalised to mock at 2 hpi. For statistical comparisons at each time point in (a, c-g, i-l) One-way ANOVA with Dunnett's post-test was used to compare groups as indicated. In (b), a Kruskal-Wallis test was used to compare groups at 24 hpi. Mean+/-SEM or individual datapoints are shown. hpi, hours post infection. $p<0.05$; **, $p<0.01$; ***, $p<0.001$; n.s., not significant.

Figure 4

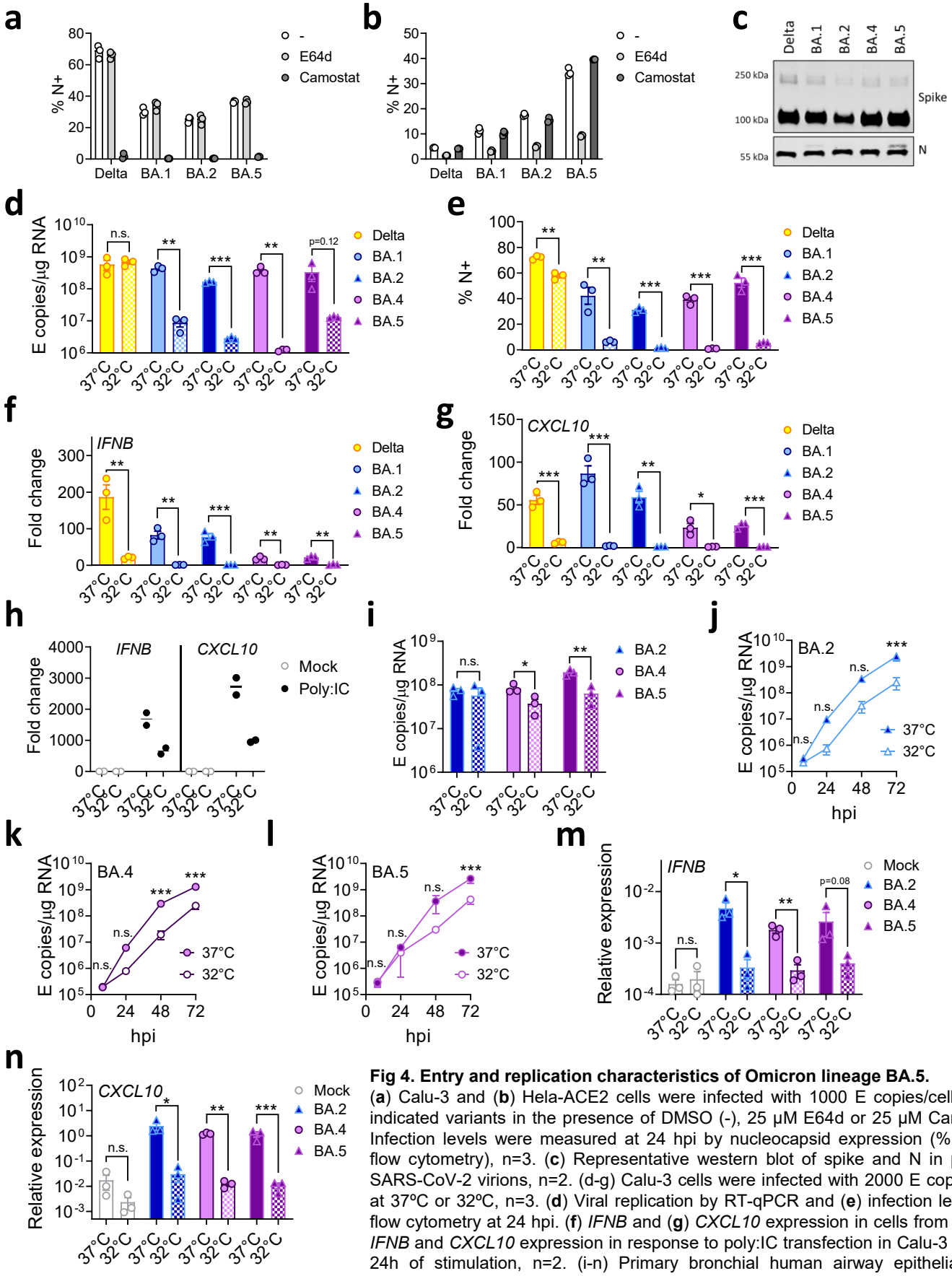

Fig 4. Entry and replication characteristics of Omicron lineage BA.5. (**a**) Calu-3 and (**b**) Hela-ACE2 cells were infected with 1000 E copies/cell of the indicated variants in the presence of DMSO (-), 25 µM E64d or 25 µM Camostat. Infection levels were measured at 24 hpi by nucleocapsid expression (% N+ by flow cytometry), n=3. (**c**) Representative western blot of spike and N in purified SARS-CoV-2 virions, n=2. (d-g) Calu-3 cells were infected with 2000 E copies/cell at 37ºC or 32ºC, n=3. (**d**) Viral replication by RT-qPCR and (**e**) infection levels by flow cytometry at 24 hpi. (**f**) *IFNB* and (**g**) *CXCL10* expression in cells from (d). (**h**) *IFNB* and *CXCL10* expression in response to poly:IC transfection in Calu-3 cells at 24h of stimulation, n=2. (i-n) Primary bronchial human airway epithelial cells (HAEs) were infected with 1500 E copies/cell of the indicated variants at 37ºC or 32ºC, n=3. Viral replication was measured by (**i**) intracellular E copies at 72 hpi and viral release of (**j**) BA.2, (**k**) BA.4 and (**l**) BA.5 into apical washes over time. Relative expression of (**m**) *IFNB* and (**n**) *CXCL10* normalised to *GAPDH* in cells from (i). Fold changes are normalised to mock. Pairwise comparisons were performed using a Student's t-Test as indicated. Mean+/-SEM or individual datapoints are shown. hpi, hours post infection. *, p<0.05 ; **, p<0.01; ***, p<0.001; n.s., not significant or exact p-value given (k).

Figure S1

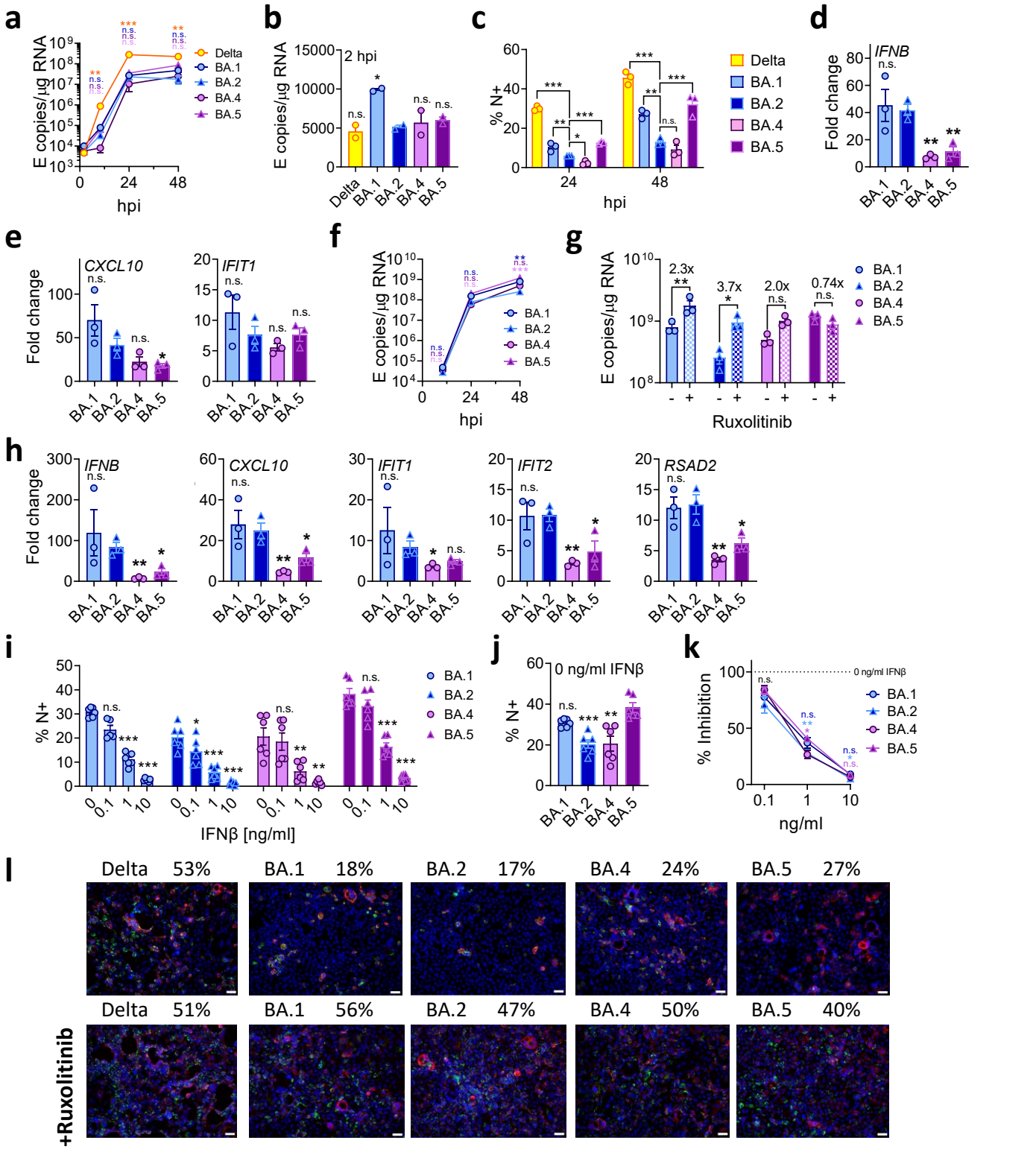

Fig S1. BA.5 displays enhanced innate immune antagonism during infection of airway epithelial cells.
(a-e) Calu-3 infection with 200 E copies/cell of Delta (orange; O), BA.1 (blue; O), BA.2 (blue; Δ), BA.4 (purple; O) and BA.5 (purple; Δ), n=3. (**a**) Viral replication over time measured by RT-qPCR for intracellular E copies. (**b**) Viral E copies at 2hpi in cells from (a). (**c**) Infections levels measured by nucleocapsid expression (% N+ by flow cytometry). Expression (**d**) *IFNB* or (**e**) *CXCL10* and *IFIT1* in infected cells at 24 hpi, n=3. (f-h) Calu-3 infection with 2000 E copies/cell of indicated variants, n=3. (**f**) Viral replication over time, n=3. (**g**) Viral replication of indicated variants in Calu-3 cells in the presence or absence of 5µM Ruxolitinib at 48 hpi, n=3. (**h**) *IFNB*, *CXCL10*, *IFIT1, IFIT2, RSAD2, MX1, MX2* and *DDX58* expression at 24 hpi, n=3. (i-k) IFNβ-sensitivity of indicated variants during Calu-3 cell infection at 2000 E copies/cell. (**i**) Infection levels measured by % N+ at 24 hpi at the indicated concentrations of IFNβ, n=6. (**j**) Infection levels in cells from (i) at 0 ng/ml IFNβ, n=6. (**k**) Infection levels from (i) normalised to 0 ng/ml IFNβ for each variant, n=6. (**l**) Fluorescence microscopy of Calu-3 cells infected at 2000 E copies/cell at 48 hpi in the presence or absence of 5µM Ruxolitinib. Percentage infection quantified by dsRNA-positive cells is indicated per condition. Representative images shown. Scale bar, 50 µm. (d, e, h). Fold changes are normalised to mock at 24 hpi. For statistical comparisons at each time point in (a-c, f, i-k), One-way ANOVA with Dunnett's post-test was used to compare BA.2 with other variants. For (a, f) colours indicate comparator (Delta, yellow; BA.1, blue; BA.4, purple; BA.5, pink). For (d, e, g, h), pairwise comparisons were performed using a Student's t-Test as indicated. Mean+/-SEM or individual datapoints are shown. hpi, hours post infection. *, p<0.05 ; **, p<0.01; ***, p<0.001; n.s., not significant.

Figure S2

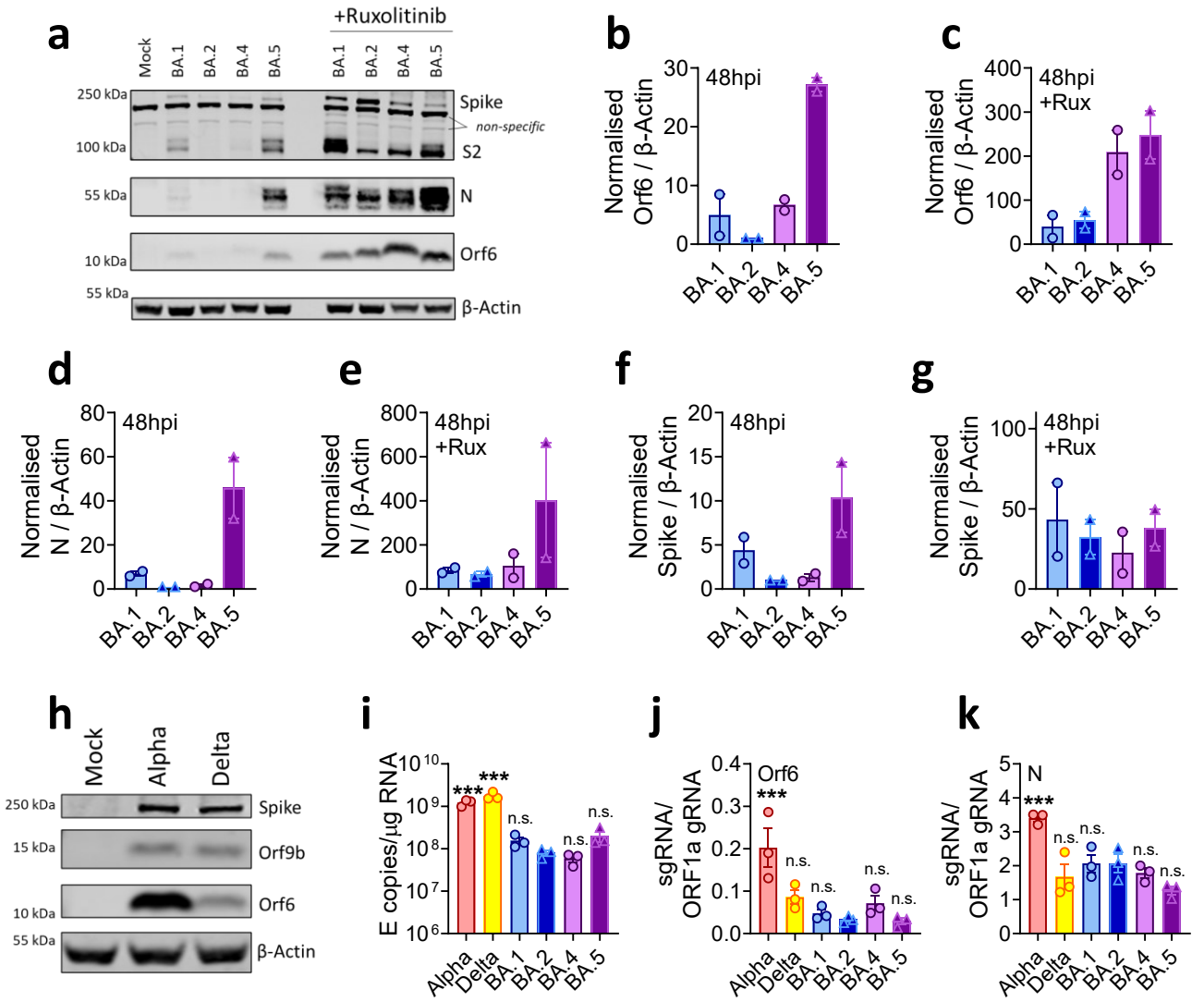

Fig S2. BA.5 efficiently expresses SARS-CoV-2 innate antagonists during airway epithelial cell infection.
(**a**) Western blot of Orf6, N, spike/S2 and β-Actin at 48 hpi in infected Calu-3 cells +/- 5µM Ruxolitinib. Non-specific bands detected by polyclonal anti-spike primary antibody are indicated. Densitometry quantification of western blots in (a) and Fig. 2 a of (**b, c**) Orf6, (**d**, **e**) N and (**f**, **g**) spike+S2 normalised to β-Actin over BA.2 at 48 hpi, n=2. (**h**) Western blot of Orf9b, Orf6, spike and β-Actin at 24 hpi in infected cells. (**i**) Viral replication by RT-qPCR at 24 hpi, n=3. (**j**) Orf6 and (**k**) N sgRNA expression in cells from (i), n=3. For (i, j, k) One-way ANOVA with Dunnett's post-test was used to compare BA.2 with other variants. Mean+/-SEM or individual datapoints are shown. hpi, hours post infection. sgRNA, subgenomic RNA. *, $p<0.05$; ***, $p<0.001$; n.s., not significant.

Supplementary Table S1. Orf6 mutations detected in the Omicron sub-lineages

	BA.1	BA.2	BA.4	BA.5
A27259C (synonymous)	+	+	+	–
G27382C, A27383T, T27384C (non-synonymous: D61L)	–	+	+	–

Presence of Orf6 mutations in BA.1, BA.2, BA.4 and BA.5 at the indicated positions compared to the reference sequence hCoV-19/Wuhan/WIV04/2019 (WIV04) (EPI_ISL_402124). Nucleotide and (non-synonymous amino acid) changes indicated. No mutations were detected in the region of the M gene surrounding the Orf6 TRS at position 27041-27046 (core TRS ACGAAC).

Supplementary Table S2. Nucleocapsid (N) mutations detected in the Omicron sub-lineages

	BA.1	BA.2	BA.4	BA.5
C28311T (non-synonymous: P13L)	+	+	+	+
A28330G (synonymous)	–	–	–	+
A28363T (synonymous)	+	+	+	+
Deletion 28364-28372 (31-33del)	+	+	+	+
C28682T (non-synonymous: P151S)	–	–	+	–
G28881A, G28882A (non-synonymous R203K[1])	+	+	+	+
G28883C (non-synonymous G204R[1])	+	+	+	+
A29510C (non-synonymous S413R)	–	+	+	+

Presence of N mutations in BA.1, BA.2, BA.4 and BA.5 at the indicated positions compared to the reference sequence hCoV-19/Wuhan/WIV04/2019 (WIV04) (EPI_ISL_402124). Nucleotide and (non-synonymous amino acid) changes indicated. BA. 1, BA.2, BA.4 and BA.5 carry nucleotide substitution A28271T, changing their Kozak initiation context from adequate (A in −3, T in +4) to the weak (T in −3, T in +4) as previously described[15]. [1] The non-synonymous mutations G203K-G204R confer a partial TRS for N* sgRNA[15].